3D Printed Light-Responsive LCE Based Soft Arm with Honeycomb Topology

24-673 Final Project Report

Team Members: Haolin Liu[1], Sen Lin[2], Jingyi Zou[2], Chenxi Wang[1]

***Abstract*:** The property of actuation responding to external stimuli has been widely studied recently and been harnessed in the field of soft robotics. Liquid crystal elastomer (LCE) has gained more attention than other types of soft actuators due to its property of reversible transformation. To date, a large variety of fabrication approaches, including three-dimensional (3D) printing, have been implemented on LCE manufacturing, aiming to reduce the difficulty of physical prototyping and enhance the accessibility of deformation programming. However, seldom insights are given regarding the material behavior of the 3D printed LCE at specific light illuminations. In this project, we design and computationally study a light-responsive 3D printed soft arm with the honeycomb topology based on the material of LCE. Based on the morphing mechanism of heat-induced phase transition, we derive a theoretical model describing the relationship between the temperature, the nematic order and the strain based on the Landau free energy theory. At last, we systematically evaluate the performance of the designed soft arm from both numerical and theoretical perspectives.

1. Introduction

Smart actuation has gained advantages of environmental-responsive, autonomous triggering and simplified structure, making it an extremely popular research area in the field of soft robotics [1,2]. Specifically, shape memory materials like shape memory alloy (SMA) and shape memory polymers (SMP) are leveraged to establish the actuator system with a large variety of geometric patterns or design topologies [1,3]. However, with the weaknesses of high fabrication cost and one-time transformation, the functionality of these material designs is considerably limited. Liquid crystalline elastomer (LCE) not only enables the feature of reversible transformation (shown in Figure 1), but also reduces the fabrication difficulty of additive manufacturing by its time-variant viscosity. Thus, three-dimensional (3D) printing LCE is tremendously developed in the aspects of medical devices, biomimetic actuators, and even untethered robotics [1,4,5].

A successful actuator system establishment should not only leverage the functionality of actuatable materials, but also rely on its topological design. Among a large variety of geometric structures, the honeycomb pattern is capable of minimizing structure's weight-to-stiffness ratio and enhancing structure's overall in-plane mechanical properties (e.g. stability, compressive stiffness, etc.) [6]. In addition, the honeycomb structure enlarges the material's deformation range through cumulating small local deformations and overall structural transforming (shown in Figure 2a), making it an optimal topology candidate for LCE assembly. However, the limited dimension of 3D printed structures and the difficulty of accurate pointwise triggering make the application of 3D printing hexagonal LCE impractical. Therefore, to verify the idea and provide more insights into the material design ahead of the experimental implementation, more work should be done regarding the theoretical analysis and computational modeling of the honeycomb LCE's mechanical behaviors.

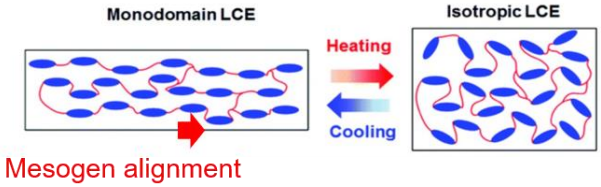

Fig. 1 Heat-induced phase transition [4], where the nematic order parameterizes the degree of mesogen alignment.

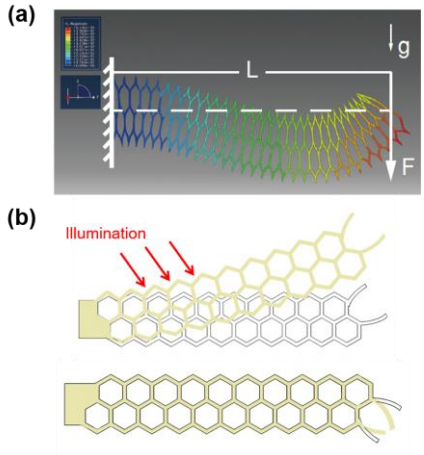

Fig. 2 (a) The simulation result of the structural deformation of a honeycomb pneumatic network [7]. (b) The inspired light responsive soft arm design based on the honeycomb topology.

In this project, we aim to design and computationally study a light responsive LCE soft arm with the honeycomb topology (shown in Figure 2b). We mainly focus on the theoretical model establishment of the LCE mechanical behavior and the finite element modeling of the honeycomb topology. We di-

[1] Department of Mechanical Engineering, Carnegie Mellon University, Pittsburgh, PA 15213
[2] Department of Electrical and Computer Engineering, Carnegie Mellon University, Pittsburgh, PA 15213

vide our project into three tasks: (1) Establishing the mathematical relationship between the temperature, the nematic order and the shrinking strain; (2) Conducting the stationary simulation based on several assumptions and simplifications; (3) Evaluating the soft arm's performance from different perspectives.

2. Methodology

2.1 Assumptions & Simplifications

To simplify the model, we make the following assumptions:

1. We assume the material is linear elastic. The nonlinear elastic behavior and viscoelastic behavior will not be considered in this project.
2. We assume the perfect connection between nearby hexagon edges. The gap between nearby printing layers and nearby hexagons will also be ignored.
3. We assume the loss during the light-to-heat energy conversion is ignorable. We merely consider the energy successfully converted to the heat from light.
4. We assume 100% light transparency of the LCE, which means there will be no light decaying and no temperature gradient along with the thickness direction.
5. We assume the heat transmission process and all the material properties are time independent.

2.2 Theoretical Modeling

2.2.1 Nematic Order Parameter

The deformation of LCE is mainly attributed to the change of mesogen alignment. With the increase of temperature, the alignment will change from perfectly nematic to nematic and eventually switch to the isotropic phase (Figure 3). To numerically describe the tendency of alignment, we introduce the nematic order parameter Q, which is an average of the second-order Legendre polynomial, $\langle P_2(cos\theta)\rangle = \langle \frac{3}{2}\, cos^2\theta - \frac{1}{2}\rangle$ [8] . The nematic order parameter can be experimentally measured by room temperature X-Ray Diffraction (XRD), in which the wide-angle X-ray scattering peak reflects the orientation of the mesophase [9].

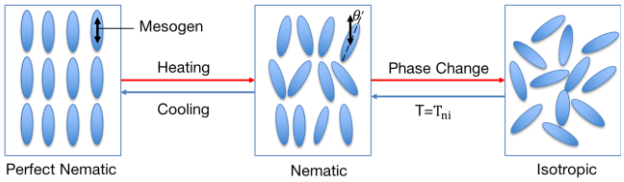

Fig. 3 The alignment of mesogen in LCE. The black arrow indicates the nematic order orientation. θ is the angle between nematic order orientation and the principal axis of a certain mesogen.

In the actual situation, the nematic order parameter is tensorial in character, and its tensor form, $\underline{\underline{\boldsymbol{Q}}}$, can be extended from the scalar form Q. If unit vector **n**= (0,0,1) represents the nematic orientation (along z-direction here), unit vector **u** represents the mesogen principal axis, and (θ, φ) represents the azimuthal angle, the projection of **u** should be $u_x = sin\theta cos\varphi, u_y = sin\theta sin\varphi, and\ u_z = cos\theta$. $\underline{\underline{\boldsymbol{Q}}}$ can thus be written as $Q_{ij} = \langle \frac{3}{2} u_i u_j - \frac{1}{2}\delta_{ij}\rangle$.

Because

$$\langle u_x u_x\rangle = \langle u_y u_y\rangle = \frac{1-\langle cos^2\theta\rangle}{2} = \frac{1-Q}{3},$$

The tensor matrix of $\underline{\underline{\boldsymbol{Q}}}$ can be represented by Q as

$$\underline{\underline{\boldsymbol{Q}}} = \begin{bmatrix} -\frac{Q}{2} & 0 & 0 \\ 0 & -\frac{Q}{2} & 0 \\ 0 & 0 & Q \end{bmatrix}.$$

The general, Landau-de Gennes expansion of the system free energy in powers of $\underline{\underline{\boldsymbol{Q}}}$ is

$$\begin{aligned} F_{nem} &= \frac{1}{3} ATr\left(\underline{\underline{\boldsymbol{Q}}} \cdot \underline{\underline{\boldsymbol{Q}}}\right) - \frac{4}{9} BTr\left(\underline{\underline{\boldsymbol{Q}}} \cdot \underline{\underline{\boldsymbol{Q}}} \cdot \underline{\underline{\boldsymbol{Q}}}\right) \\ &\quad + \frac{2}{9} CTr\left(\underline{\underline{\boldsymbol{Q}}} \cdot \underline{\underline{\boldsymbol{Q}}} \cdot \underline{\underline{\boldsymbol{Q}}} \cdot \underline{\underline{\boldsymbol{Q}}}\right) + \cdots \\ &= \tfrac{1}{2} AQ^2 - \tfrac{1}{3} BQ^3 + \tfrac{1}{4} CQ^4 + \cdots \end{aligned}$$

When the system achieves thermodynamic equilibrium, the free energy should be at a minimum, which requires

$$\frac{\partial F_{nem}}{\partial Q} = 0 \;\&\; \frac{\partial^2 F_{nem}}{\partial Q^2} > 0\,,$$

From which we can obtain the formula of Q with several unknown parameters:

$$Q_m(T) = \begin{cases} \frac{1}{2C}\left(B \pm \sqrt{B^2 - 4A_0(T - T_s)C}\right) (T \le T_{ni}) \\ 0\ (T > T_{ni}) \end{cases},$$

In which T_{ni} and T_s are the first- and second-order phase transition temperature, respectively.

We then fit the formula into the experimental data of LCE [10], and the result is shown in Figure 4. From the fitted curve, we can also calculate some critical values of the material, including the phase change temperatures T_{ni} = 360.15K, T_s =356.20 K, and phase change nematic order Q_{ni} =0.14.

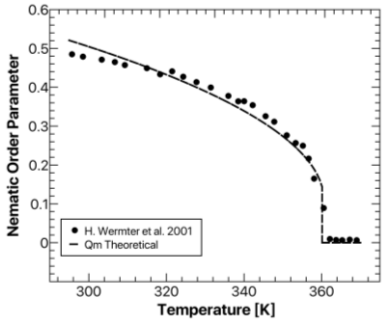

Fig. 4 The experimental data (from [10]) and simulation results of the nematic order parameter- temperature relationship.

2.2.2 Thermal Strain

We apply two methods to describe the trend of stretch change with temperature.

Method 1: Approximation. We find from the experimental data that the nematic order- temperature relationship and relative length (stretch)- temperature relationship, is quite similar in shape, and their difference of value is around 1. Based on this, we can make the approximation that $\lambda = \mathrm{L(T)}/L_{iso} \approx Q(T) + 1$ to obtain our strain, where L_{iso} represents the length of the elastomer at isotropic phase along the direction of orientation **n**. The dashed black line in Figure 5a shows that the approximated stretch fits well with the experimental data. To further evaluate our approximation, Figure 5b plots the direct relationship between the stretch and nematic order parameter, and the fitting of the data points exhibits a linear relationship $y = 0.987x + 1.014$ (dashed black line), which is close to our approximation. Due to limited experimental data access, we cannot determine whether this relationship is applicable to other liquid crystalline elastomers; but for the specific nematic material measured in [10], the error of the approximation is acceptable.

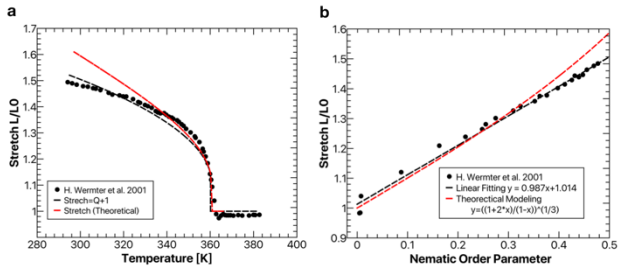

Fig. 5 (a)(b) Change of natural length of a monodomain nematic elastomer with temperature and nematic order parameter, respectively. The experimental data is collected from [10]. The dashed black line represents the stretch calculated by the approximation approach. The dashed red line represents the stretch calculated from the theoretical model.

The thermal strain, which is the change of length relative to the natural length at room temperature, is then calculated according to the stretch and applied in our COMSOL simulation.

Method 2: Freely Jointed Chain Model. Apart from the approximation of stretch, we also present a theoretical approach to calculating the relationship between stretch and nematic order parameter. A freely jointed chain model is applied to describe the deformation of the polymer chain (As shown in Figure 6). The parameters used in the model are listed in Table 1.

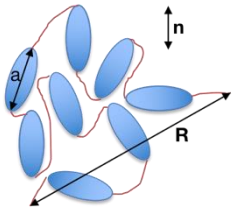

Fig. 6 Illustration of the freely jointed chain model. The blue ellipses represent the mesogen, and the red line is the simplified structure of the spacer that connects between each mesogen.

Table 1 Parameters mentioned in the freely jointed chain model

PARAMETERS	DESCRIPTION
a	Natural length of monomer at isotropic phase
$\boldsymbol{l}$	Effective step length
L	Overall arc length
$\boldsymbol{R}$	End-to-end distance
N	Number of mesogen
$\boldsymbol{u_\alpha}$	The orientation of α^{th} mesogen
r	Anisotropy

A few assumptions are made before the derivation. First, we consider the LC polymer to be main chain, i.e., each mesogen is connected directly to the backbone of the polymer. Second, the elastomer formed is incompressible in volume, which is a typical characteristic of materials with relatively low shear moduli. Third, the LC polymer is in the uniaxial nematic phase. In a freely jointed chain model, we also assume that the physical properties of the total system depend weakly on its detailed structure, which means that the entanglement and constraints of the chains are neglected.

The end to end distance R, which reflects the macroscopic shape of the polymer, can be written as

$$\boldsymbol{R} = a \sum_{i=1}^{N} \boldsymbol{u_\alpha}.$$

The mean square end-to-end vector can thus be described in the form of effective step length, which is calculated from random walk theory [11].

$$\langle \boldsymbol{R_i R_j} \rangle = \frac{1}{3} L l_{ij}.$$

As a result, the effective step length tensor can be written as

$$\underline{\underline{\boldsymbol{l}}} = \begin{bmatrix} l_\perp & 0 & 0 \\ 0 & l_\perp & 0 \\ 0 & 0 & l_\parallel \end{bmatrix} = \frac{3}{Na} \langle \boldsymbol{RR} \rangle = \frac{3a}{N} \sum_{\alpha,\beta} \langle \boldsymbol{u_\alpha u_\beta} \rangle = 3a \langle \boldsymbol{uu} \rangle.$$

Apply the same method used to calculate tensor $\underline{\underline{\boldsymbol{Q}}}$ and get

$$\underline{\underline{\boldsymbol{l}}} = \begin{bmatrix} l_\perp & 0 & 0 \\ 0 & l_\perp & 0 \\ 0 & 0 & l_\parallel \end{bmatrix} = 3a \begin{bmatrix} \frac{\langle sin^2\theta \rangle}{2} & 0 & 0 \\ 0 & \frac{\langle sin^2\theta \rangle}{2} & 0 \\ 0 & 0 & \langle cos^2\theta \rangle \end{bmatrix} = a \begin{bmatrix} 1-Q & 0 & 0 \\ 0 & 1-Q & 0 \\ 0 & 0 & 1+2Q \end{bmatrix}.$$

As can be seen, the effective step length has a closer relationship with the microscopic nematic order Q. The chain anisotropy is therefore defined to be the ratio of step length parallel to the director and that perpendicular to the director,

$$r = \frac{l_\parallel}{l_\perp} = \frac{1+2Q}{1-Q}.$$

At this point, we have related the step length with the nematic order parameter. To further derive the stretch-nematic order relation, a Neo-Hookean elasticity model is applied to calculate $\lambda - l$ relation. When the liquid crystal elastomer is at the isotropic phase, it tends to appear spherical with the absence of external fields because of symmetry along different orientations. When the temperature decreases, the stretch is going to happen along the direction parallel to the director **n**, while in the other two perpendicular orientations the length will shrink. The stretch tensor can be described as

$$\lambda_\parallel = \lambda = \frac{L}{L_0}, \lambda_\perp = \frac{1}{\sqrt{\lambda}}.$$

According to [8], the elastic free energy density of liquid crystalline elastomer is a coupling of stretch and step length, which can be written in the form of:

$$F(\lambda) = \frac{1}{2}\mu Tr[\boldsymbol{l_0} \cdot \boldsymbol{\lambda}^T \cdot \boldsymbol{l^{-1}} \cdot \boldsymbol{\lambda}] = \frac{1}{2}\mu \mathrm{Tr} \begin{bmatrix} \frac{a}{\lambda l_\perp} & 0 & 0 \\ 0 & \frac{a}{\lambda l_\perp} & 0 \\ 0 & 0 & \frac{a\lambda^2}{l_\parallel} \end{bmatrix} = \frac{1}{2}\mu \left(\frac{2a}{\lambda l_\perp} + \frac{a\lambda^2}{l_\parallel} \right),$$

In which μ is the shear modulus of the material, $\boldsymbol{l_0} = a\boldsymbol{\delta_{ij}}$ is the length of mesogen before the deformation, and $\boldsymbol{l^{-1}}$ is the inverse of the step length tensor during the deformation.

Similar to the nematic free energy, we let the first derivation of $F(\lambda)$ to be 0 and find

$$\lambda_m = \left(\frac{l_\parallel}{l_\perp} \right)^{\frac{1}{3}} = (r)^{\frac{1}{3}}.$$

Consequently, the stretch-nematic order parameter relation appears to be

$$\lambda(Q) = \left(\frac{1+2Q}{1-Q} \right)^{\frac{1}{3}}.$$

The dashed red lines in Figure 5 reflects the performance of this model. This model fits well with experimental data at the low-Q region but predicts a higher value of stretch at the high-Q region. Two factors might contribute to the phenomenon. First, in the freely jointed chain model we assumed that no constraint is posed to the alignment of the mesogen, but in fact at the high-Q region, the spacers and crosslinks will play a more important role and thus cannot be neglected. Additionally, the material tested in [10] is a side-chain polymer, in which the chain conformational freedom is affected by the linkages to the backbone and the volume fraction of the rods in the polymer [12].

3. Results & Discussion

3.1 Key parameters

In this section, a series of simulation experiments are conducted to explore the relationship between actuator temperature and performance (flexural rigidity, load capacity, flexibility vs. light power & heat distribution). Specifically, the parts of the manipulator composed of 20 to 40 regular hexagonal units are created using COMSOL MULTYPHYSICS as shown in Figure 7. We set Young's modulus as 750 kPa, Poisson's rate as 0.44, density as 851 kg/m^3, thermal conductivity as 0.238 W/(m*K) and heat capacity as 1618 J/(kg*K) for the liquid crystalline elastomer (LCEs) of the frame [13][14].

As shown in Figure 7, a fixed constraint is applied on one side of the arm which is called fixed end. Correspondingly, the other end of the arm is called the free end. The total length and width of the arm are 66 mm and 14 mm respectively. The thickness of the arm is from 0.5 mm to 5 mm. It depends on the limitation of the existing LCE 3D printing technology, which is relatively difficult to print thick LCE structure. But in our simulation, we partially ignore this limitation to explore the potential of this design.

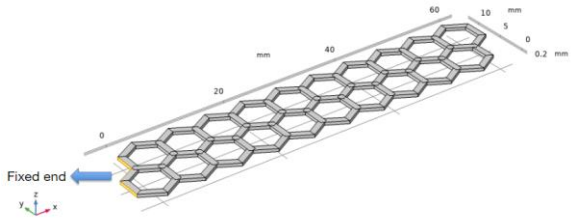

Fig. 7 Sketch of the honeycomb arm and geometric constraint relationship

3.2 Flexibility

We use two criterions to characterize the flexibility of the LCE actuator, the displacement of the yellow point at the free end as the tip displacement and the angle transition of the LCE actuator calculated by the coordinates of the red point and the yellow point as the tip displacement. Sketch of test settings are shown in Figure 8.

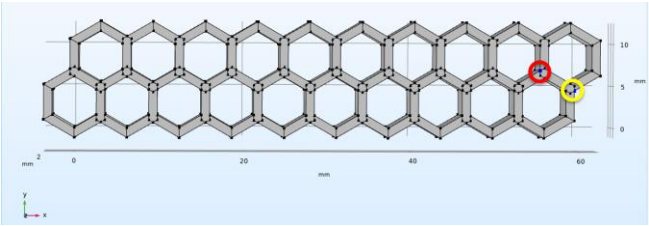

Fig. 8 settings for deformation test

Deformation of the actuator and distribution of temperatures are shown in Figure 9.

The statistic results are shown in Figure 10(a) and Figure 10(b). Both curves are linear at beginning. They transit to nonlinear phases right after the excitation reaches 1 W and then saturate quickly at roughly 120 degrees and 40 mm after 1.25 W excitation. The non-linear effects are believed to most be the result of the non-linear phenomenon of the relative length and temperature characteristic of LCE.

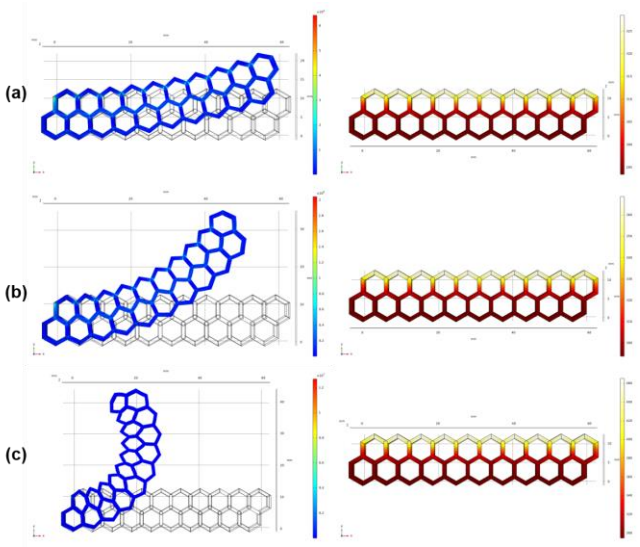

Fig. 9 The left figure column indicates the deformation under heating power of 0.5W, 1.0W, and 2.0W from (a) to (c) respectively. The right figure shows the corresponding temperature distribution.

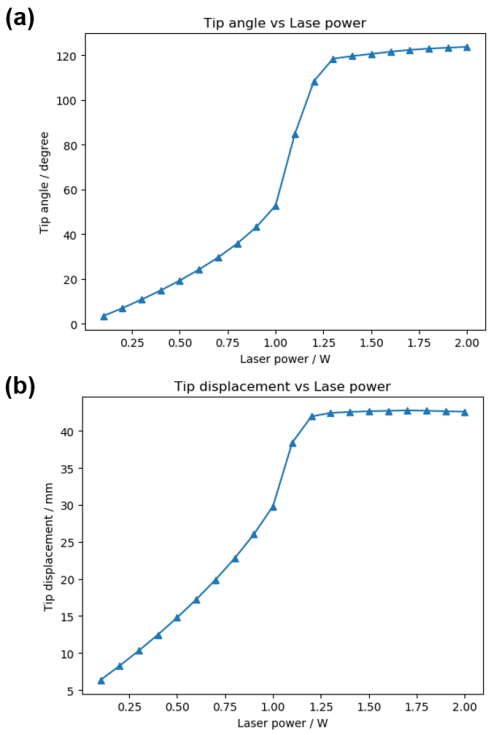

Fig. 10 (a) Tip angle vs. laser power (b) Tip displacement vs. laser power

3.3 Flexural Rigidity

The flexural rigidity is characterized by a test where the LCE actuator is fixed at both side and force load is applied at the center of the LCE actuator as shown in Fig. 11 and Figure 12. For a beam structure, the flexural rigidity is just EI, where E

is the Young's modulus and *I* is the second moment of inertia. In this case, it is not appropriate to consider the LCE actuator as a beam given the elasticity and honeycomb structure it has. Therefore, we conduct a modified three-point test and use the displacement of the center to characterize the flexural rigidity. In this experiment, we set the thickness of the actuator in z direction as 0.5 mm.

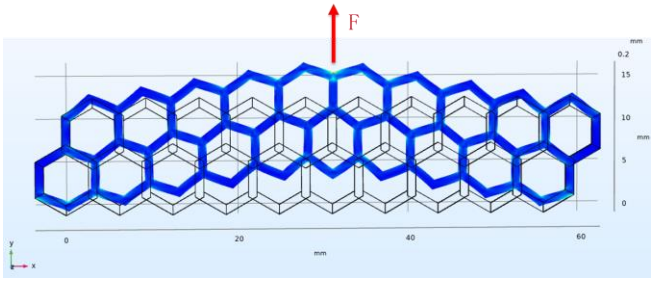

Fig. 11 Flexural rigidity test setup in y axis. The left and right ends of the actuator are fixed. Force is applied as shown in the figure. No heat excitation is applied to the actuator.

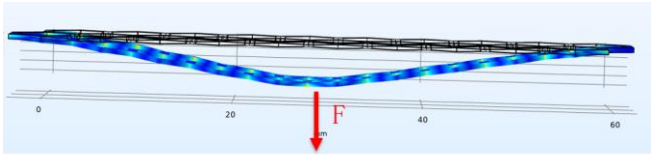

Fig. 12 Flexural rigidity test setup in z axis. The left and right ends of the actuator are fixed. Force is applied as shown in the figure. No heat excitation is applied to the actuator.

The results are shown in Figure 13(a) and Figure 13(b) The curve of deflection vs. force load in y direction is near linear. The force load reaches almost 10mN when the deformation comes to 4 mm. Consider that the self-weight of the LCE actuator is 0.12 mg, the force load at the end of the curve is nearly 10 times of its self-weight load. The average deflection to force load ratio is 5.15 m/N.

On the contrast, the curve for z direction has significant nonlinear effect. Given the same force load, the deflection in z direction is also remarkably smaller than the one in y direction. The average deflection to force load ratio is 77.36 m/N.

To summarize, the flexural rigidity in y direction is higher than the flexural rigidity in z direction. The reason can be the lack of thickness in z direction. In fabrication, achieving large thickness in z direction is still a challenging work.

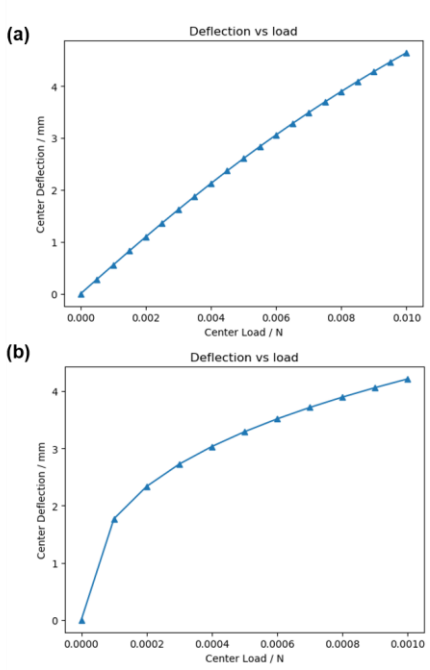

Fig. 13 (a) Flexural rigidity in y direction; (b) Flexural rigidity in z direction.

3.4 Load Capacity

There are several ways to achieve the condition that the tip and the fixed end of the manipulator are on the same height under a load. Here we choose the evaluation method shown in Figure 14. All the lines of LCE are heated to 370 K on the higher side and its load increases until the two ends reach the same height. *F* represents the external load. The honeycomb arm moves in a horizontal plane. The simulation result shows that load capacity of the arm is about four times its own weight. As shown in Figure 15, the load capacity is proportional to arm thickness. Therefore, we expect that when the thickness of the arm reaches the same order of magnitude (centimeter-level) as the width of the arm, not only its load capacity can be improved by nearly a hundred times, but its ability to resist undesired twisting and buckling will also be greatly improved.

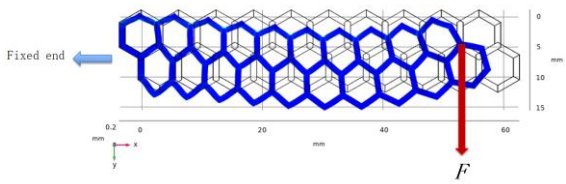

Fig. 14 Sketch of the principle of measuring the load capacity of the honeycomb arm.

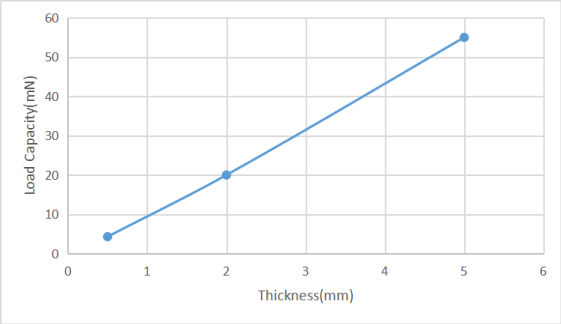

Fig. 15 Load capacity of arm at different thickness

3.5 Structural deformation vs. Light (heat) distribution

The proposed honeycomb topology is supposed to achieve multiple configurations by varying the heating region (illuminated region) upon the LCE. As depicted in Figure 16, since the designed soft arm bends towards the direction of the heating region, we can manipulate its overall in-plane bending behavior by controlling the side of the heating region (top or bottom). With proper illumination distribution, the soft arm can reach curved shape (Figures 16a and 16c), S-shape (Figure 16b), and a wavelike shape (Figure 16d).

4. Conclusion & Future work

In this project, we propose and study a light responsive LCE soft arm with the honeycomb topology. We firstly establish a theoretical relationship between the shrinking and the temperature, then we simulate the light-induced mechanical behavior of the LCE soft arm based on the aforementioned assumptions and simplifications, and finally we systematically evaluate the soft arm's performance from different perspectives. We explore the potential application values of the honeycomb topology based LCE actuator system in advance of experimental verification, aiming to providing insights into the honeycomb LCE design.

This project has a huge room for improvement. We summarize the future work into four aspects:

Simulation. Since LCE is a typical viscoelastic material, we may consider its viscoelasticity and damping behavior in the future and include them into the simulation model. We may include the inhomogeneous light intensity distribution into the simulation, especially the light decaying along with the thickness direction, which may result in shrinking strain gradient perpendicular to the design plane. We may also explore transient simulations, regarding the material property and the heat transmission process as functions of time.

Theoretical modeling. Based on the established relationship between the nematic order, the temperature and the shrinking strain, we may further derive the relationship between the local shrinkage and the arm's total bending deflection.

Design. In the future, we may include more geometric patterns into our soft arm design, i.e. triangles, squares, and octagons. A more complex topology may achieve more deformed configurations and further carry more functionalities.

Experimental implementation. We may develop this project with accurate material characterization of LCE. We can improve the fabrication technique and LCE recipe to generate more stable and robust printing of large structures. We may explore possible dyes for LCE so as to achieve efficient light-to-heat energy conversion. If the size of the designed soft arm is large enough, we may integrate optical fibers into it to achieve precise deformation control by accurately delivering the light to each single hexagon edge.

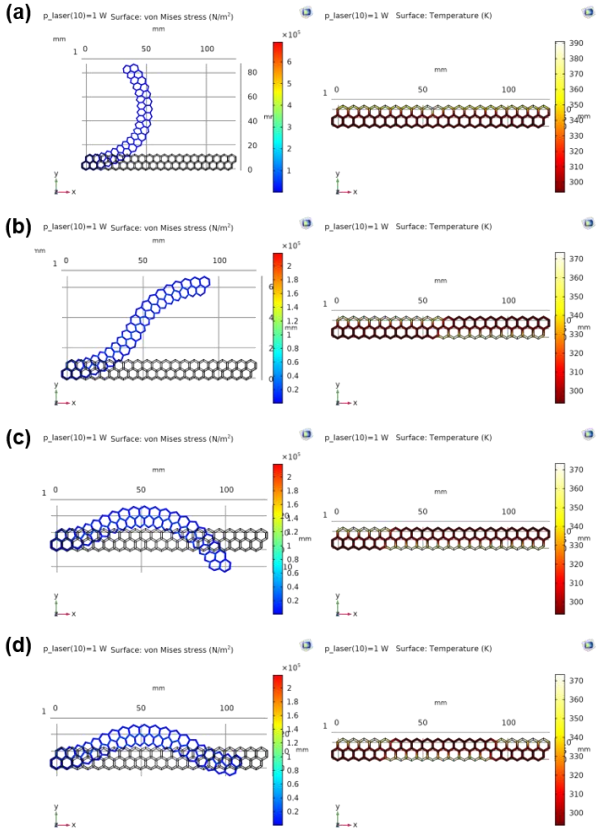

Fig. 16 Deformed patterns with different heating regions (illuminated edges distribution). The left column indicates the stress distribution on the deformed structure, and the right column indicates the temperature distribution under corresponding illumination. The heating regions are: (a) all top edges; (b) 1/2 top edges (top left) + 1/2 bottom edges (bottom right); (c) 1/4 top edges (top left) + 3/4 bottom edges (bottom right); (4) 1/4 top edges (top left) + 1/2 bottom edges (bottom middle) + 1/4 top edges (top right), respectively.

Acknowledgement

We would like to express our special thanks to Prof. Carmel Majidi, the instructor of the course 24-673A in Spring 2020, and TAs of the course, who instructed us on the cutting-edge knowledge in soft robotics and gave us many suggestions and inspiration throughout the project implementation. We acknowledge Prof. Lining Yao, the principal investigator of Morphing Matter Lab at Human-Computer Interaction Institute, Carnegie Mellon University, who gave us support and help during the beginning period of this project. We are thankful to Kuanren Qian, master student from the Department of Mechanical Engineering, Carnegie Mellon University, who instructed us and cooperated with us in 3D printing manipulation. Especially thanks for Prof. M. Ravi Shankar, Dr. Arul Clement and the research team from the Department of Industrial Engineering, University of Pittsburgh, who provided us with the LCE printing recipe and all necessary chemical materials at the beginning.

References

[1] Majidi, Carmel. "Soft-matter engineering for soft robotics." Advanced Materials Technologies 4.2 (2019): 1800477.
[2] Wani, Owies M., Hao Zeng, and Arri Priimagi. "A light-driven artificial flytrap." Nature communications 8.1 (2017): 1-7.
[3] Rodrigue, Hugo, et al. "An overview of shape memory alloy-coupled actuators and robots." Soft robotics 4.1 (2017): 3-15.
[4] Yuan, Chao, et al. "3D printed reversible shape changing soft actuators assisted by liquid crystal elastomers." Soft Matter 13.33 (2017): 5558-5568.
[5] Davidson, Emily C., et al. "3D printable and reconfigurable liquid crystal elastomers with light-induced shape memory via dynamic bond exchange." Advanced Materials 32.1 (2020): 1905682.
[6] Wang, Zhonggang, Jiefu Liu, and David Hui. "Mechanical behaviors of inclined cell honeycomb structure subjected to compression." Composites Part B: Engineering 110 (2017): 307-314.
[7] Jiang, Hao, et al. "Design and simulation analysis of a soft manipulator based on honeycomb pneumatic networks." 2016 IEEE International Conference on Robotics and Biomimetics (ROBIO). IEEE, 2016.
[8] M. Warner and E. M. Terentjev, “Liquid crystal elastomers,” Oxford University Press, vol. 120, pp. 9-20, Apr., 2007.
[9] S. Dey et al. “Soft elasticity in main chain liquid crystal elastomers,” Crystals, vol. 3, no. 2, pp. 363-390, Jun., 2013.
[10] H. Wermter, and H. Finkelmann, "Liquid crystalline elastomers as artificial muscles," E-Polymers, vol. 1, no. 1, Dec., 2001.
[11] P. J. Flory, “Principles of polymer chemistry”, Cornell University Press, 1953.
[12] V. P. Shibaev, S. G. Kostromin, and N. A. Plate,” Thermotropic liquid-crystalline polymers-VI: Comb-like liquid-crystalline polymers of the smectic and nematic types with cyanobiphenyl groups in the side-chains”, European Polymer Journal, vol. 18, no. 8, pp. 651-659, 1982.
[13] M. L. Dunn, “Photomechanics of mono- and polydomain liquid crystal elastomer films,” Appl. Phys., vol. 102, no. 1, pp. 013506, Jul, 2007.
[14] S. Ge, T. Zhao, M. Wang, “A homeotropic main-chain tolane-type liquid crystal elastomer film exhibiting high anisotropic thermal conductivity,” Soft Matter, vol. 13, no. 1, pp. 5463-5468, Jul, 2017.